Amylose folding under the influence of lipids

Lopez, Cesar A.; de Vries, Alex H.; Marrink, Siewert J.

Published in:
Carbohydrate Research

DOI:
10.1016/j.carres.2012.10.007

Publication date:
2012

Carbohydrate Research 364 (2012) 1–7

Contents lists available at SciVerse ScienceDirect

Carbohydrate Research

journal homepage: www.elsevier.com/locate/carres

Amylose folding under the influence of lipids

Cesar A. López *, Alex H. de Vries, Siewert J. Marrink

Groningen Biomolecular Sciences and Biotechnology Institute & Zernike Institute for Advanced Materials, University of Groningen, Nijenborgh 7, 9747 AG Groningen, The Netherlands

ARTICLE INFO

Article history:
Received 3 July 2012
Received in revised form 4 October 2012
Accepted 6 October 2012
Available online 17 October 2012

Keywords:
Molecular dynamics
Carbohydrates
Oligosaccharides
V-Amylose
Protein folding

ABSTRACT

The molecular dynamics simulation technique was used to study the folding and complexation process of a short amylose fragment in the presence of lipids. In aqueous solution, the amylose chain remains as an extended left-handed helix. After the addition of lipids in the system, however, we observe spontaneous folding of the amylose chain into a helical structure, with helical pitch and hydrogen bond network compatible with the V-amylose structure observed in X-ray experiments. Our results suggest that under the influence of external non polar ligands, the conformation of amylose undergoes a transition from an extended to a V-amylose structure in line with experimental evidence.

1. Introduction

Amylose is a linear [α 1→4] linked polymer and the principal component of starch. In aqueous solution, it behaves as a flexible random coil with stretches of left-handed helical segments that are more pronounced at low hydration levels.[1] Stable secondary conformations, known as A-, B- and V-amylose, are formed in either ionic solutions or less polar solvents.[2] The A- and B-allomers consist of parallel left-handed double helices with six glucopyranosyl units per turn, differing only in the number of helices packed in the unit cell. V-Amylose, co-crystallized with compounds such as iodine, DMSO, or alcohols, reveals a stable left-handed helix, stabilized by six to eight glucoses per turn. Multiple helices form a central channel in which the additives are complexed.[3] In fact different arrangements are observed in the unit cell for V-amylose crystals, depending on the exact crystallization conditions.[4]

Amylose can also fold under the influence of other compounds, such as surfactants and lipids. The amylose–lipid complexes are important in the food industry[5] (e.g., emulsifying starch) and are suitable nanocapsules for controlled release of lipids. Despite their importance, characterization of the structural and dynamical properties of these complexes at the molecular level is still lacking. Amylose–lipid complex formation is known to be affected by degree of polymerization of amylose, pH, complexation temperature and the structure of the complexed lipid.[6] It has also been shown that the thermal stability of the amylose–fatty acid complex is highly dependent on the aliphatic chain length as well as the level of saturation.[7] Theoretical considerations suggest that V-amylose forms an imperfect helix with the aliphatic tails positioned inside, and the lipid head group outside the helix. The position of the carboxyl groups at the linkage between the lipid head and tail is still controversial.[8,9]

Molecular dynamics (MD) simulations have proven to be a useful tool for providing a link between dynamics and structure. Many force fields have been extensively parameterized for carbohydrates,[10–17] and have been used to provide details of the structure and dynamics at an all atom (AA) level; for example to explore the ring puckering of glucose,[18,19] conformational changes in disaccharides and trisaccharides.[11,20–22] However, previous MD studies of amylose have mainly dealt with small amylose fragments in water or studies of V-amylose in low polarity solvents.[23–25]

The object of the present study was to deepen the understanding of the structure and formation of V-amylose inclusion complexes in view of its anticipated use as a delivery system of long chain fatty acids and other nutraceuticals. To that aim, we consider a short amylose fragment, and simulate its structure and dynamics in the presence of either dipalmitoyl-phosphatidylcholine (diC_{16}-PC) or glycerol monooleate (GMO) in aqueous solution. We observe that, over a time period of 400 ns, the presence of either lipid induces a hydrophobic collapse of the amylose chain resulting in the formation of a stable V-amylose–lipid inclusion complex.

The rest of this paper is organized as follows. The method section gives details about the simulation approach and free energy calculations. Subsequently, the results are presented in three parts. The first part concerns a slight adjustment of the GROMOS carbohydrate force field in order to reproduce the experimentally observed structure of amylose in excess water and the stability of V-amylose in apolar solvents. The second part describes the structure formation and characteristics of amylose chains in apolar

* Corresponding author. Tel.: +31 (050) 363 4457; fax: +31 (050) 363 4800.
E-mail address: C.A.Lopez-Bautista@rug.nl (C.A. López).

0008-6215/$ - see front matter © 2012 Elsevier Ltd. All rights reserved.
http://dx.doi.org/10.1016/j.carres.2012.10.007

solvents, followed by the complexation of amylose with lipids in the third part. A short conclusive section ends this work.

2. Methods

2.1. Force field details

All computations were carried out with the GROMOS force field parameter set for carbohydrates,[16] with a slight modification in the charge distribution of the hydroxyl groups required to reproduce the experimental behavior of amylose chains in aqueous solvent (see Section 3). In particular, the negative charges on the O_3, O_2 and O_6 atoms were increased from −0.642 to −0.842, while the positive charges of the HO_3, HO_2 and HO_6 were increased from 0.41 to 0.61 (see Fig. 1A and B). The adjusted set of parameters can be found as part of the Supplementary data.

The lipids diC_{16}-PC and GMO as well as nonane and butanol were modeled using the parameters for aliphatic hydrocarbons that are part of the GROMOS 53a6 force field.[26] For the water molecules, the simple point charge model (SPC)[27] was applied.

2.2. Simulation protocol

Newton's equations of motion were integrated with the Gromacs[28] MD package, using a 2 fs time step. The LINCS algorithm[29] was applied to constrain all bond lengths, note that this approach was considered in the original parameterization of the force field.[16] The temperature was maintained at 300 K by weak coupling of the solvent and solute separately to a Berendsen heat bath[30] with relaxation times of 0.1 ps. The pressure was maintained at 1.0 bar by weak coupling to a pressure bath via isotropic coordinate scaling with a relaxation time of 1 ps. Non-bonded interactions were handled using a twin-range cut-off scheme.[31] Within a short-range cut-off of 0.9 nm, the interactions were evaluated every time step based on a pair list recalculated every 5 time steps. The intermediate-range interactions up to a long-range cut-off radius of 1.4 nm were evaluated simultaneously with each pair list update, and assumed constant in between. To account for electrostatic interactions beyond the long-range cut-off radius, a reaction field approach[32] was used having a relative dielectric permittivity of 66 for water, 2 for nonane, and 17 for butanol. After a short energy minimization, the systems were simulated for 400 ns and the atomic coordinates were stored every 400 ps for analysis.

2.3. Folding simulations

Two types of simulations were performed. The first type consisted of a 26-mer amylose chain placed in a cubic box of size $14 \times 14 \times 14$ nm filled either with 8460 nonane or 54,000 water molecules. The starting structure of these simulations was a fully stretched chain generated using the GLYCAM server (http://www.glycam.com). Before production time, the internal energy of the chain was minimized using a steepest descent algorithm.[28] Afterward, these simulations were run for 100 ns and were aimed at obtaining the equilibrium structure of the amylose chain in both polar and apolar environment.

The second type of system consisted of a shorter, 13-mer amylose chain in order to study the complexation with lipids. The amylose chain was either pre-complexed with a lipid (diC_{16}-PC or GMO), or the amylose and lipid chain were put in separately to observe spontaneous complexation. In the former case, the amylose chain was initially in a V-amylose conformation and the lipid tail(s) were inserted into the helical channel. In case of diC_{16}-PC, simulations were initiated with either a single or both tails inside the channel. In the spontaneous complexation simulations, the amylose chain was put in in a stretched, open conformation, and the lipid was placed randomly in the box. A reference simulation of the short amylose chain without lipid was also performed. In each case, the system was embedded in a cubic box of $6 \times 6 \times 6$ nm^3 volume and filled with between 7000 and 7500 water molecules. The complexation process was studied over time scales up to 400 ns.

2.4. PMF calculation

To test the accuracy of the force field currently used in this work, we set up calculations in order to reproduce experimental data available. Thus, two types of PMF (Potential of Mean Force)

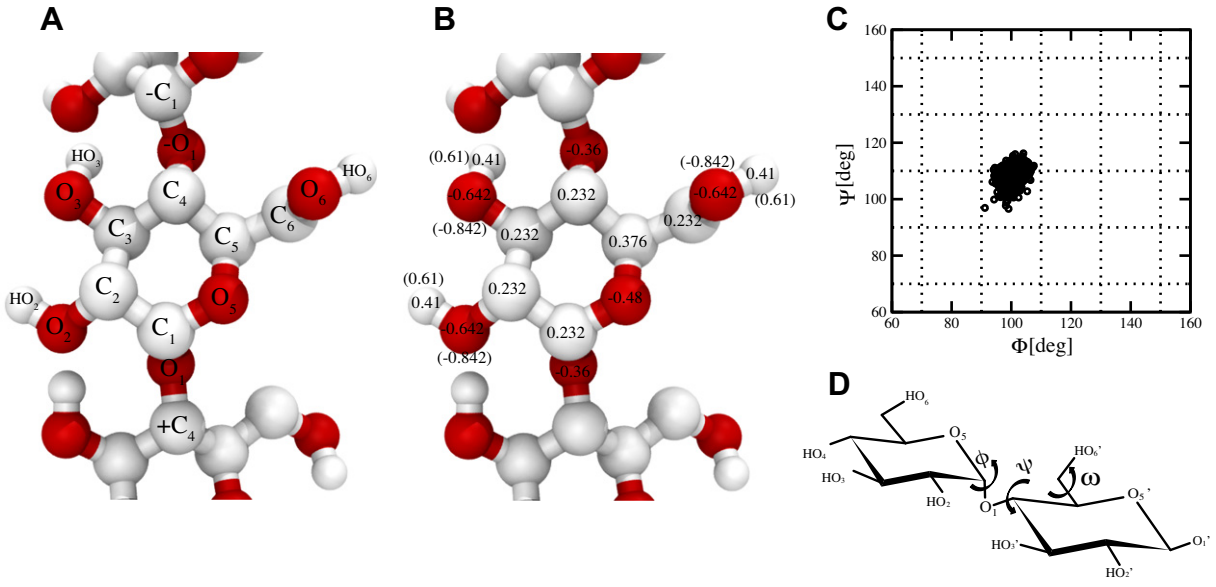

Figure 1. Amylose topology according to the GROMOS force field.[16] (A) and (B), indication of partial charge distribution according to the GROMOS force field as well as the modifications applied (in parenthesis). (C) Distributions of the ϕ (O_5–C_1–O_1–C'_4) and ψ (C_1–O_1–C'_4–C'_3) glycosidic dihedral angles for the 26-mer amylose chain in water. Successive points are reported at a frequency of 40 ps. (D) Indication of atom names and torsional angles (φ, ψ) described in this work.

calculations were performed: (i) stretching of a short helical amylose fragment in butanol using steered-MD to reproduce experimental AFM force spectrograms, and (ii) computation of the equilibrium free energy for unwinding of helical amylose, also in butanol.

To simulate the unfolding of V-amylose mimicking an AFM experiment, we placed a 13-mer pre-folded V-amylose in a rectangular box of dimensions (x, y, z) $4 \times 5 \times 4$ nm, with the amylose helical axis along the y-dimension. The box was subsequently filled with 500 butanol molecules. Unfolding of the amylose chain was forced using a steered molecular dynamics (SMD) approach as follows: The atoms (C_5–O_5–C_1–O_1) from the nonreducing end were position restrained to avoid tumbling or tilting of the molecule during the simulation. The atoms (C_5–O_5–C_1–O_1) from the reducing end were restrained using an harmonic umbrella potential[33] with a force constant of 1000 kJ mol^{-1} nm^{-2}, which moved at a speed of 0.000001 nm ps^{-1} in the direction of the helical axis during 1 μs.

To compute the equilibrium free energy associated with the unfolding process of V-amylose, an umbrella sampling approach[33] was used. The system is the same as for the SMD case. Thus, 25 window points spaced by 1 Å were used, restraining the center of mass of the reducing end with respect to the nonreducing end of the amylose chain. The restraining (umbrella) potential was harmonic with a force constant of 1000 kJ mol^{-1} nm^{-2}. Simulations were performed over 400 ns for each window. The PMFs were reconstructed using the Weighted Histogram Analysis Method (WHAM),[34] with 200 bins for each profile. To estimate the convergence in the PMF, each window trajectory was divided into blocks. The statistical error was calculated from the variance between averages over individual blocks, using a block averaging procedure. Blocks were found to be statistically independent over 20 ns time intervals.

2.5. Clustering analysis

In order to find representative clusters of structures in the simulation trajectory, we followed the procedure described by Daura et al.[35] The RMSD of atom positions between pairs of amylose structures was determined. The structure with the highest number of neighbors using a cut-off of 0.2 nm was taken as the center of a cluster. The process was repeated until the pool of structures was exhausted.

3. Results and discussion

3.1. GROMOS force field adjustment

In water, using the standard GROMOS charge distribution for hexopyranoses, the amylose chain behaves as a flexible polymer with no stable secondary structural elements (Fig. 2A). The initial left-handed helix, used as starting conformation, unfolds immediately. Water molecules interact strongly with the O_3 and O_2 of each glucose residue, breaking the intramolecular hydrogen bonding network already after a few nanoseconds. Also, we observe that several glucose residues undergo a *trans* flipping, adopting a chair $^1C_4$ conformation that drastically affects the structure of the amylose chain. From the total number of residues, 60% were found in the $^1C_4$ conformation at the end of our simulation. This is in contrast to NMR measurements for maltohexaose,[36] in which the hexopyranose rings are observed in a conserved $^4C_1$ conformation in aqueous solution. Moreover, the disruption of the internal $O_{3n}HO_{3n}\cdots O_{2n-1}$ hydrogen bond network is not in line with experimental measurements.[37–40] To overcome this problem, we decided to increase the dipole moment of the hydroxyl groups by increasing the negative charges of the O_3, O_2 and O_6 from −0.642 to −0.842 and the positive charges of the HO_3, HO_2 and HO_6 from 0.41 to 0.61. The increase of charges results in a higher strength of the $O_{3n}HO_{3n}\cdots O_{2n-1}$ hydrogen bond pairs that are responsible for maintaining the helical structure. After this modification, indeed we observe that the amylose chain shows stretches of left-handed helix with all the sugar rings in the $^4C_1$ puckering state, as depicted in Figure 2B. The presence of left-handed helical stretches is consistent with experimental data.[38]

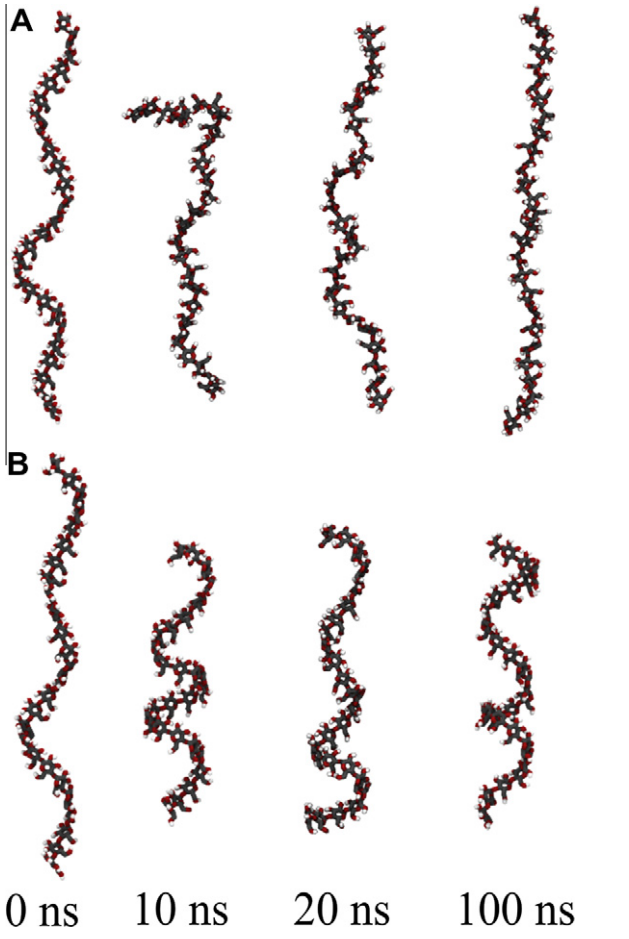

Figure 2. Conformational sampling of a 26-mer amylose chain in water. (A) A random structureless conformation is observed when standard GROMOS charges are used for the hydroxyl groups. (B) Increasing charges on the hydroxyl groups the amylose chain behaves as an extended helix with stretches of left-handed turns, consistent with experimental data.

A useful way to assess the conformation of the amylose chain is by determining the populations of rotamers around the glycosidic linkage (represented by the φ and ψ dihedrals, Fig. 1D). The distribution of φ (O_5–C_1–O_1–C'_4) and ψ (C_1–O_1–C'_4–C'_3) obtained for the simulation of the amylose strand in water is shown in

Table 1
Average value for φ, ψ dihedral angles and population around ω dihedral as extracted from the simulations of amylose in water

	φ^*	$\psi*$	$\omega*$ tg/gg/gt, %[†]
$Amylose_{water}$	71.88° (±10)	94.71° (±12)	0/60/40
Maltose[a]	87.2°	100.5°	0.0/65.2/37.3
Maltose[b]	88.5°	95.5°	—
Maltose[c]	94.7°	106.1°	5/71/24

[a] and [b]MD data were taken from Pereira[22] and Ott[41]. [c]NMR data were taken from Cheetham et al.[42]

[†] Population around ω was defined as tg = 180°, gg = 60° and gt = −60°.

[*] For definition of these angles, see Figure 1. Standard deviations are reported in parenthesis.

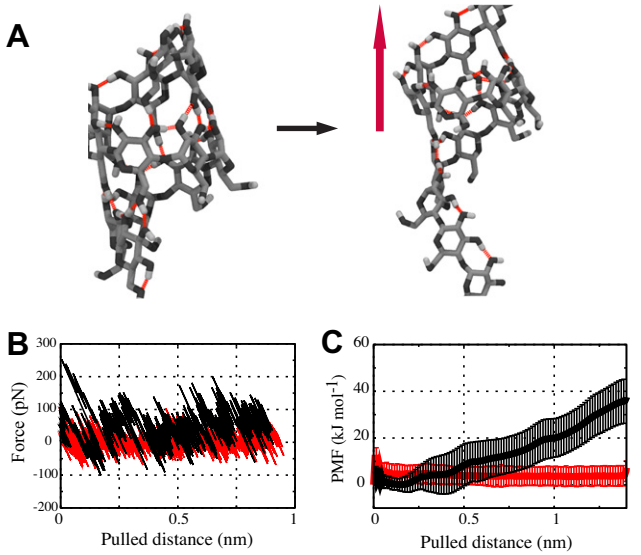

Figure 3. Simulated unwinding of a 13-mer V-amylose in butanol. (A) Initial and final snapshots of the amylose chain being partially unfolded with an external force of 1000 kJ mol^{-1} nm^{-2} (indicated by the red arrow). (B) Extension-force diagram for the unfolding of the amylose fragment. Standard GROMOS charges in red, modified charges in black. (C) Potential of mean force (PMF) for unfolding of the V-amylose chain in butanol, with GROMOS (red) or modified (black) charge distribution. (For interpretation of the references to color in this figure legend, the reader is referred to the web version of this article.)

Figure 1C. The average values of these dihedrals are reported in Table 1 and are close to those obtained from other MD simulations,[22,41] NMR[42] and X-ray experiments[43,44] of maltose dimers and NMR data for cyclodextrins,[45] suggesting that the relative orientation of the sugar rings does not change much when the helical chain is elongated. In line with this, our results are also in good agreement with experimental measurements for amylose chains in solution as well as for branched carbohydrates.[37–40]

In order to test our new parameter set in non-aqueous environment, we tried to reproduce experimental AFM force spectrograms obtained for several amylose chains in butanol.[46] We used a steered-MD approach to mimic the AFM experiment as explained in Section 2. The simulated partial unwinding process of the amylose chain in butanol is illustrated in Figure 3A, depicting the initial and final structures. The extension reached at the end of the pulling was nearly 1.0 nm and forced the breaking of the hydrogen bonds responsible for the stabilization of one turn of the V-amylose chain. The simulated force–extension curve of amylose is shown in Figure 3B for both the standard GROMOS charges and the modified charge distribution model. The standard parameters fail to reproduce the experimental unfolding strength of amylose in butanol, which requires about 50 pN after an initial stretching phase of the amylose chain.[46] Using the modified version of the force field, the force required to initiate unfolding is about 50 pN (±5 pN), matching the experimental value.

To explore the folding process from an energetic point of view, we calculated the PMF for the unwinding of one helical turn of the same V-amylose chain solvated in butanol. We compare the PMF profiles for the standard and modified charge models (Fig. 3C). The almost flat profile obtained with the original GROMOS charges indicates that the folded conformation is not stable using the standard parameters. On the other hand, the unfolding of the amylose with the modified charges is unfavorable by nearly 40 ± 8 kJ mol^{-1}. This is consistent with experimental data showing a stable V-amylose fold in solvents of low polarity.[46,1] Considering that the new set of charges better reproduces the conformation and energetics of amylose observed experimentally, we decided

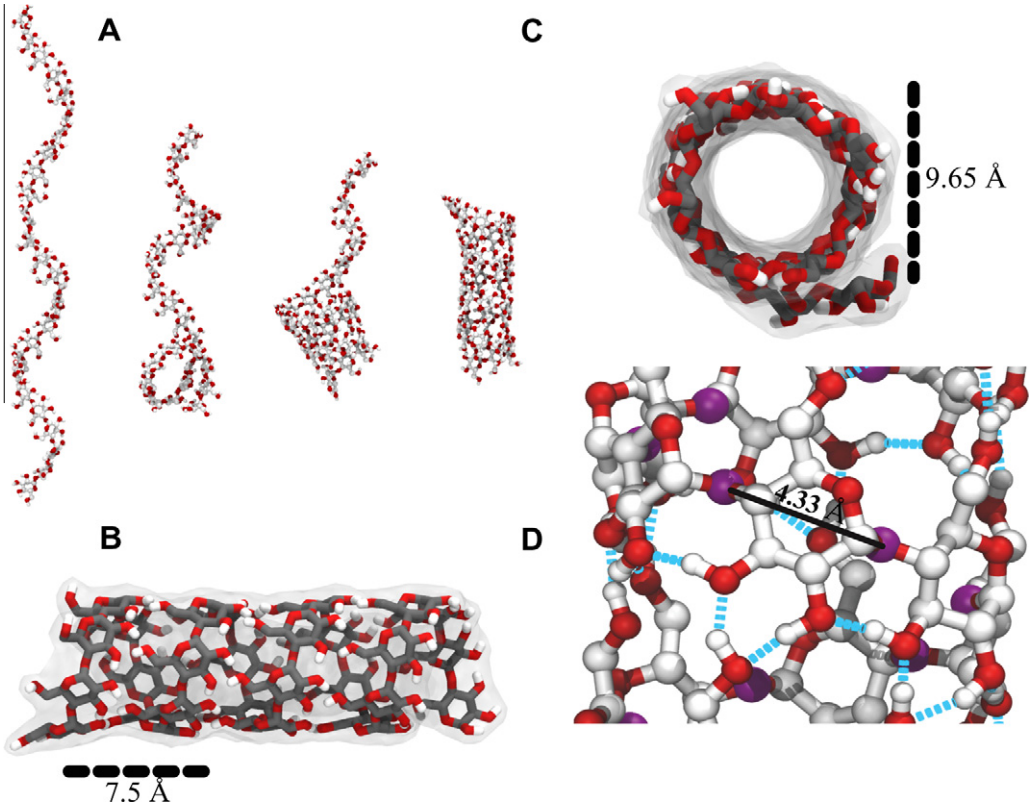

Figure 4. Folding of a 26-mer amylose chain into a V-amylose structure in nonane. (A) Snapshots from the folding process taken over a time-span of 100 ns. (B–D) Final structure of spontaneously folded V-amylose, with indication of the internal pitch value for two consecutive turns (B), the mean value of the diameter of the helical conformation (C), and h-bonding network with average O_{1n}–O_{1n+1} distance.

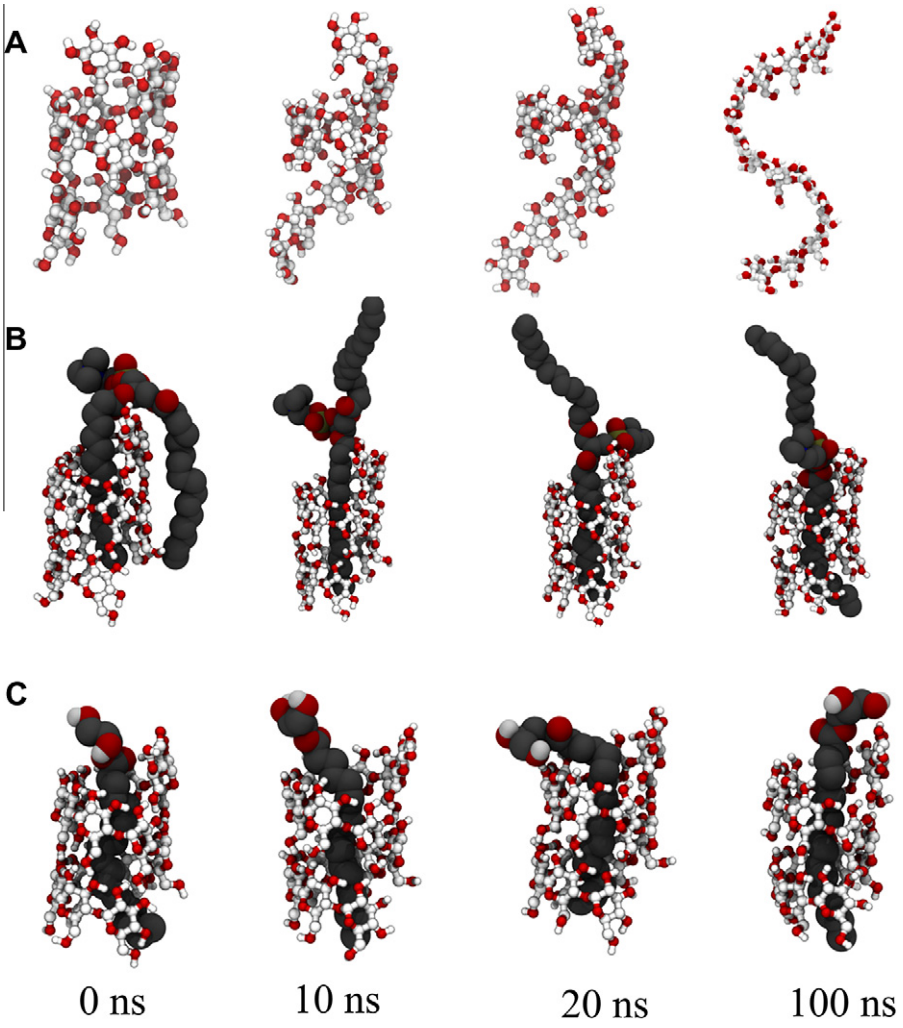

Figure 5. V-Amylose is stable in water when complexed with lipids. Snapshots taken from simulations of a 13-mer amylose chain alone (A), showing unfolding, or in complex either with diC_{16}-PC (B) or GMO (C) revealing a stable V-amylose conformation.

to keep using them for the remainder of this work. Note that an improved GROMOS-based carbohydrate force field[19] has recently been released that might remedy some of the issues observed here.

3.2. Structure and folding of amylose in nonane

In contrast to the extended left-handed helix observed in aqueous solution, the simulation of a 26-mer amylose chain in nonane converged to a well-defined helical structure which is comparable to the V-amylose crystal structures previously reported.[47] Figure 4A shows snapshots of this process. The global structure of the V-amylose chain, as obtained in our simulations, is depicted in Figure 4B–D. The chain is characterized by a pitch length of 7.5 Å, corresponding to 7 glucoses per pitch, and an average diameter of 9.65 Å based on the distance O_{3n}–C_{5n+3}. In the experimentally resolved crystal structures, the diameter is highly dependent on the molecule which is included inside the channel. For instance, V-amylose molecules co-crystallized with butanol have a diameter of 8.1 Å, while in complex with isopropanol they range from 9.1 to 9.5 Å.[3] The difference in experimental diameter might be related to the ability of solvent molecules to enter the channel-like cavity inside the helix. In the simulation at least three nonane molecules are included in the heilx; these molecules continuously pass through the channel and are replaced by new molecules. The complexing of linear alkane molecules inside the hydrophobic cavity has been confirmed experimentally,[48] consistent with our findings. The average value for O_{1n}–O_{1n+1} distance is 4.33 Å in most of the structure while at the non-reduced end of the chain this value is 4.65 Å. These values are close to those obtained from the crystal structure of a 26 residues cycloamylose (4.39 Å), the biggest V-amylose fragment crystallized until now.[47] Another feature of the structure is the presence of all the glucoses in the *syn* conformation with φ and ψ = 105° and 104° respectively. The torsion angle ω for the C_5–C_6 hydroxymethyl group is in the preferred *gg* (*gauche–trans*) conformation with a mean value of −84.2°. The glucose residues are in the common $^4C_1$ conformation as observed in the V-amylose crystal.[47]

3.3. Amylose structure in complex with lipids

To provide a molecular view on the structure and dynamics of amylose-lipid complexes, we simulated a short 13-mer V-amylose fragment pre-complexed with a single lipid, either the single tail GMO or double tail diC_{16}-PC. The same amylose fragment without a lipid was also simulated for reference. Snapshots from these simulations are shown in Figure 5. In the uncomplexed state, the short V-amylose chain used as starting conformation unfolds rapidly to a more extended conformation; like the 26-mer (cf. Fig. 2B) preserving stretches of left-handed helix. In contrast, the amylose chain with either diC_{16}-PC or GMO embedded preserves its well-defined

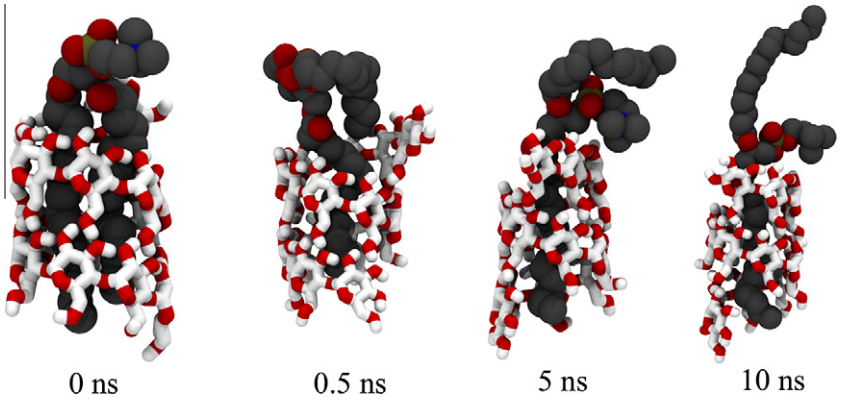

Figure 6. V-amylose structure limits the size of the bound ligand. Starting from a V-conformation (0 ns), both aliphatic tails of diC_{16}-PC were inserted inside the hydrophobic channel. However, one tail is rapidly expelled (0.5 ns), leaving only a single tail inside the hydrophobic core (10 ns).

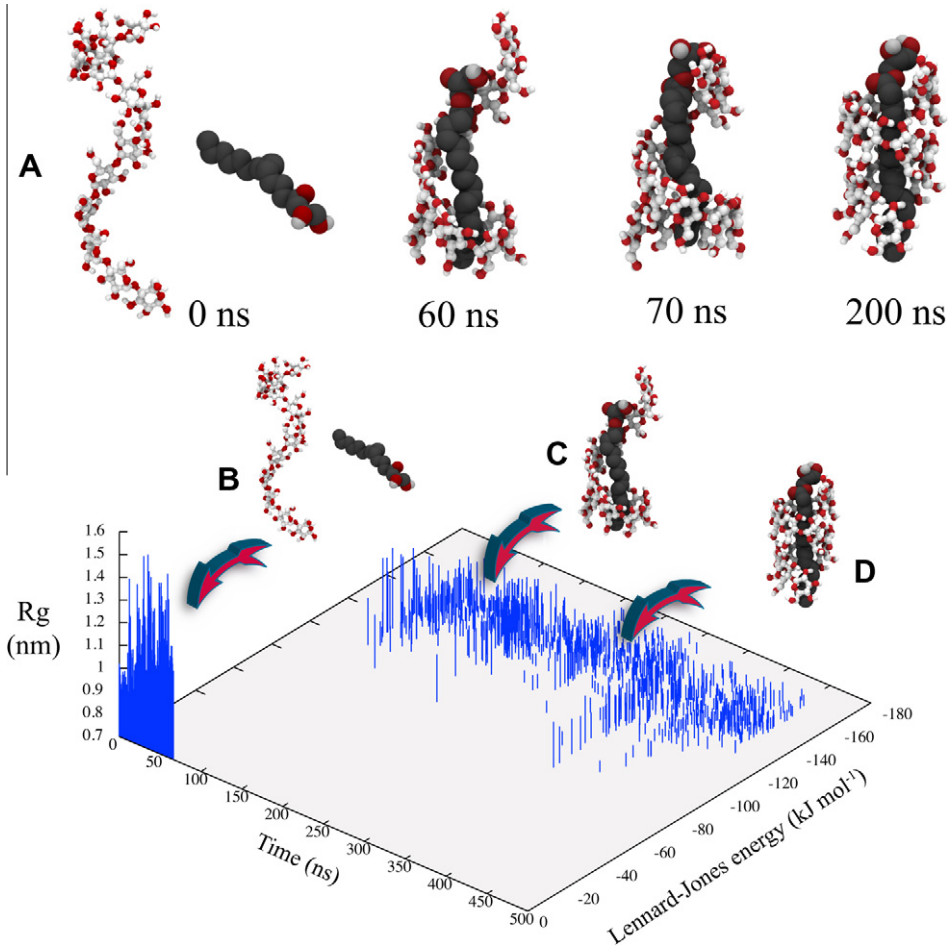

Figure 7. Folding transition of amylose after complexation with GMO. Starting from an extended helical conformation (A), the polysaccharide undergoes a transitional conformation to a compact V-structure (200 ns). A cluster analysis based on the radius of gyration, Rg, and internal Lennard-Jones energy shows three well defined structures during the complexation process: uncomplexed (B), complexed but unfolded (C), and complexed V-shape (D).

helical structure which is comparable to the V-amylose crystal structure discussed above for amylose in nonane. The complexes are stable during the entire simulation trajectory (400 ns) without further transitions (Fig. 5B and C). In the case of diC_{16}-PC, we started from a conformation in which only one of the two lipid tails resides in the V-amylose channel. Starting from a conformation in which both aliphatic tails of the diC_{16}-PC are inserted, the simulation converged to a structure in which only one tail is complexed, as shown in Figure 6. Apparently, the diameter of V-amylose (9.65 Å) does not allow the complexation of bulkier compounds. Our findings, observed in several independent simulations, agree with experimental detection of linear alkane molecules inside the V-amylose hydrophobic cavity[48] and complexation studies between different lipids and the polysaccharide.[49]

Having shown that a single lipid tail is sufficient to stabilize V-amylose in otherwise aqueous conditions, we next attempted to simulate the actual folding process upon complexation. To this end, we started from an unfolded 13-mer amylose fragment in close vicinity to a GMO lipid, mimicking the contact pair which could have formed following a stochastic diffusional process.

Indeed, during a 400 ns simulation we observe the spontaneous complexation of GMO and concomitant folding of amylose into V-amylose. The whole process is depicted in Figure 7. Starting from an extended left-handed helix, the GMO molecule interacts with the channel-like structure of amylose (60 ns). After the complexation, the amylose chain showed a fast collapse, folding toward the V-amylose state within a time period of 200 ns.

To analyze the folding pathway in more detail, we performed a structural clustering analysis.[35] We classified the clusters with respect to the radius of gyration (Rg) and the GMO-amylose Lennard-Jones interaction. Based on this classification, three (meta)stable states can be discerned as depicted in Figure 7. State 1 (panel B) covers the unfolded amylose chain, which is constituted of elongated left-handed conformations and characterized by a high Rg and virtually zero LJ interaction with GMO. State 2 (panel C) shows the GMO-amylose complexation, with the amylose chain undergoing a rapid collapse. This state already has the correct diameter, but is still partly unfolded especially toward both ends. The final conformation, state 3 (panel D), is reached after 200 ns of simulation and corresponds to the stable V-amylose structure. From these results it is clear that a hydrophobic collapse (due to the interaction of the aliphatic chain with the monosaccharide rings) triggers the conformational change and stabilizes the V-conformation of amylose in aqueous conditions.

4. Conclusion

In this work, we studied the conformational behavior of small amylose chains either free in solution or in complex with lipids. After an ad hoc optimization of the force field, we observed that in a polar solvent like water, a single strand of amylose behaves as an elongated left-handed chain, due principally to the disruption of the inter-residual hydrogen bonds. In contrast, after the addition of lipids, the amylose chain undergoes a conformational change to a V-amylose, driven principally by the interaction of the aliphatic lipid-tails with the hydrophobic core of the polysaccharide. Once formed, this complex is very stable. Our results, in line with experimental evidence, point out that the amylose is able to complex only single tail lipids.

As a spin-off of our simulation, we found that crystallization conditions of long polysaccharides can be effectively reproduced by low dielectric solvents (nonane). This is in remarkable contrast with proteins, which usually possess side chains of different polarity leading to trapped intermediates. Direct simulation of protein folding is therefore still restricted to small peptides and even then requires microsecond time scales. Our simulations show that the folding of a 26-residue amylose chain in a low polar medium is much faster, occurring on a time scale of less than 200 ns.

Appendix A. Supplementary data

Supplementary data associated with this article can be found, in the online version, at http://dx.doi.org/10.1016/j.carres.2012.10.007.

References

1. Cheetham, N. W. H.; Tao, L. *Carbohydr. Polym.* **1998**, *35*, 287–295.
2. Nuessli, J.; Putaux, J. L.; Bail, P. L.; Buléon, A. *Int. J. Biol. Macromol.* **2003**, *33*, 227–234.
3. Helbert, W.; Chanzy, H. *Int. J. Biol. Macromol.* **1994**, *16*, 207–213.
4. Cardoso, M. B.; Putaux, J.-L.; Nishiyama, Y.; Helbert, W.; Hÿtch, M.; Silveira, N. P.; Chanzy, H. *Biomacromolecules* **2007**, *8*, 1319–1326.
5. Ahmadi-Abhari, S.; Woortman, A. J. J.; Hamer, R. J.; Oudhuis, A. A. C. M.; Loos, K. *Carbohydr. Polym.* in press. http://dx.doi.org/10.1016/j.carbpol.2012.05.020.
6. Zabar, S.; Lesmes, U.; Katz, I.; Shimoni, E.; Bianco-Peled, H. *Food Hydrocolloids* **2009**, *23*, 1918–1925.
7. Kowblansky, M. *Macromolecules* **1985**, *18*, 1776–1779.
8. Godet, M. C.; Tran, V.; Delage, M. M.; Buléon, A. *Int. J. Biol. Macromol.* **1993**, *15*, 11–16.
9. Putseys, J.; Lamberts, L.; Delcour, J. J. *Cereal Sci.* **2010**, *51*, 238–247.
10. Kirschner, K. N.; Yongye, A. B.; Tschampel, S. M.; González-Outeirino, J.; Daniels, C. R.; Foley, B. L.; Woods, R. J. J. *Comput. Chem.* **2008**, *29*, 622–655.
11. Behrends, R.; Kaatze, U. *ChemPhysChem* **2005**, *6*, 1133–1145.
12. Green, D. F. J. *Phys. Chem. B* **2008**, *112*, 5238–5249.
13. Kräutler, V.; Müller, M.; Hünenberger, P. H. *Carbohydr. Res.* **2007**, *342*, 2097–2124.
14. Guvench, O.; Greene, S. N.; Kamath, G.; Brady, J. W.; Venable, R. M.; Pastor, R. W.; Mackerell, A. D. J. *Comput. Chem.* **2008**, *29*, 2543–2564.
15. Kony, D.; Damm, W.; Stoll, S.; van Gunsteren, W. F. J. *Comput. Chem.* **2002**, *23*, 1416–1429.
16. Lins, R. D.; Hünenberger, P. H. J. *Comput. Chem.* **2005**, *26*, 1400–1412.
17. López, C. A.; Rzepiela, A. J.; de Vries, A. H.; Dijkhuizen, L.; Hunenberger, P. H.; Marrink, S. J. J. *Chem. Theory Comput.* **2009**, *5*, 3195–3210.
18. Spiwok, V.; Lipovová, P.; Skálová, T.; Vondrácková, E.; Dohnálek, J.; Hasek, J.; Králová, B. J. *Comput.-Aided Mol. Des.* **2005**, *19*, 887–901.
19. Hansen, H. S.; Hünenberger, P. H. J. *Comput. Chem.* **2010**, *32*, 998–1032.
20. Stenutz, R.; Widmalm, G. *Glycoconjugate J.* **1998**, *15*, 415–418.
21. Kozar, T.; Tvaroska, I.; Carver, J. P. *Glycoconjugate J.* **1998**, *15*, 187–191.
22. Pereira, C. S.; Kony, D.; Baron, R.; Müller, M.; van Gunsteren, W. F.; Hünenberger, P. H. *Biophys. J.* **2006**, *90*, 4337–4344.
23. Tusch, M.; Krüger, J.; Fels, G. J. *Chem. Theory Comput.* **2011**, *7*, 2919–2928.
24. Yu, H.; Amann, M.; Hansson, T.; Kohler, J.; Wich, G.; van Gunsteren, W. F. *Carbohydr. Res.* **2004**, *339*, 1697–1709.
25. Kuttel, M.; Naidoo, K. J. J. *Am. Chem. Soc.* **2005**, *127*, 12–13.
26. Oostenbrink, C.; Villa, A.; Mark, A. E.; van Gunsteren, W. F. J. *Comput. Chem.* **2004**, *25*, 1656–1676.
27. Berendsen, H. J. C.; Postma, J. P. M.; van Gunsteren, W. F.; Hermans, J. *Interaction Models for Water in Relation to Protein Hydration*; Reidel: Dordrecht, 1981.
28. Hess, B.; Kutzner, C.; van der Spoel, D.; Lindahl, E. J. *Chem. Theory Comput.* **2008**, *4*, 435–447.
29. Hess, B.; Bekker, H.; Berendsen, H. J. C.; Fraaije, J. J. *Comput. Chem.* **1997**, *18*, 1463–1472.
30. Berendsen, H. J. C.; Postma, J. P. M.; van Gunsteren, W. F.; Dinola, A.; Haak, J. R. J. *Chem. Phys.* **1984**, *81*, 3684–3690.
31. van Gunsteren, W. F.; Berendsen, H. J. C. *Angew. Chem. Int. Ed.* **1990**, *29*, 992–1023.
32. Tironi, I.; Sperb, R.; Smith, P.; van Gunsteren, W. F. J. *Chem. Phys.* **1995**, *102*, 5451–5459.
33. Torrie, G.; Valleau, J. J. *Comput. Phys.* **1977**, *23*, 187–199.
34. Kumar, S.; Rosenberg, J.; Bouzida, D.; Swendsen, R.; Kollman, P. J. *Comput. Chem.* **1992**, *13*, 1011–1021.
35. Daura, X.; Gademann, K.; Jaun, B.; Seebach, D.; van Gunsteren, W. F.; Mark, A. E. *Angew. Chem., Int. Ed.* **1999**, *38*, 236–240.
36. Sugiyama, H.; Nitta, T.; Horii, M.; Motohashi, K.; Sakai, J.; Usui, T.; Hisamichi, K.; Ishiyama, J. I. *Carbohydr. Res.* **2000**, *325*, 177–182.
37. Boone, M. A.; Nymeyer, H.; Striegel, A. M. *Carbohydr. Res.* **2008**, *343*, 132–138.
38. Motawia, M. S.; Damager, I.; Olsen, C. E.; Moller, B. L.; Engelsen, S. B.; Hansen, S.; Øgendal, L. H.; Bauer, R. *Biomacromolecules* **2005**, *6*, 143–151.
39. Uccello-Barretta, G.; Sicoli, G.; Balzano, F.; Salvadori, P. *Carbohydr. Res.* **2005**, *340*, 271–281.
40. Bekiroglu, S.; Kenne, L.; Sandström, C. J. *Org. Chem.* **2003**, *68*, 1671–1678.
41. Ott, K.; Meyer, B. *Carbohydr. Res.* **1996**, *281*, 11–34.
42. Cheetham, N. W. H.; Dasgupta, P.; Ball, G. E. *Carbohydr. Res.* **2003**, *338*, 955–962.
43. Quigley, G. J.; Sarko, A.; Marchessault, R. H. J. *Am. Chem. Soc.* **1970**, *92*, 5834–5839.
44. Takusagawa, F.; Jacobson, R. A. *Acta Crystallogr. Sect. B* **1978**, *34*, 213–218.
45. Schneider, H.-J.; Hacket, F.; Rüdiger, V.; Ikeda, H. *Chem. Rev.* **1998**, *98*, 1755–1786.
46. Zhang, Q.; Lu, Z.; Hu, H.; Yang, W.; Marszalek, P. E. J. *Am. Chem. Soc.* **2006**, *128*, 9387–9393.
47. Gessler, K.; Usón, I.; Takaha, T.; Krauss, N.; Smith, S. M.; Okada, S.; Sheldrick, G. M.; Saenger, W. *Proc. Natl. Acad. Sci. U.S.A.* **1999**, *96*, 4246–4251.
48. Nimz, O.; Gessler, K.; Usón, I.; Sheldrick, G. M.; Saenger, W. *Carbohydr. Res.* **2004**, *339*, 1427–1437.
49. Snape, C. E.; Morrison, W. R.; Maroto-Valer, M. M.; Karkalas, J.; Pethrick, R. A. *Carbohydr. Polym.* **1998**, *36*, 225–237.